Title: Excessive self-grooming of *Shank3* mutant mice is associated with gene dysregulation and imbalance between the striosome and matrix compartments in the striatum

Abbreviated title:

Behavioural and transcriptomic alterations in the *Shank3*$^{\Delta 11/\Delta 11}$ mice

Author names and affiliations, including postal codes:

Ferhat Allain-Thibeault* (1,2,3), Biton Anne* (4), Verpy Elisabeth* (1), Forget Benoit (1), de Chaumont Fabrice (1), Mueller Florian (5), Le Sourd Anne-Marie (1), Coqueran Sabrina (1), Julien Schmitt (6), Rochefort Christelle (6), Rondi-Reig Laure (6), Leboucher Aziliz (1), Boland Anne (7), Fin Bertrand (7), Deleuze Jean François (7,8), Boeckers Tobias M. (9,10), Ey Elodie[#] (1,11), Bourgeron Thomas[#] (1)

* Equally contributed to the work

[#] Co senior-authors

1. Génétique Humaine et Fonctions Cognitives, Institut Pasteur, UMR3571 CNRS, Université de Paris, Paris, France

2. Department of Neuroscience, Columbia University Medical Center, New York, NY, 10027

3. Zuckerman Mind Brain Behavior Institute, Columbia University, New York, NY, 10027

4. Centre de Bioinformatique, Biostatistique et Biologie Intégrative (C3BI, USR 3756 Institut Pasteur and CNRS), Paris, France

5. Unité Imagerie et Modélisation (UMR 3691 Institut Pasteur and CNRS), Paris, France

6. Sorbonne Université, CNRS, INSERM, Institut de Biologie Paris Seine (IBPS), Neurosciences Paris Seine (NPS), Cerebellum Navigation and Memory Team (CeZaMe), F-75005 Paris, France

7. Université Paris-Saclay, CEA, Centre National de Recherche en Génomique Humaine (CNRGH), 91057, Evry, France

8. Centre d'étude du polymorphisme humain, Paris, France

9. Institute of Anatomy and Cell Biology, Ulm University, 89081 Ulm, Germany

10. Deutsches Zentrum für Neurodegenerative Erkrankungen (DZNE), 89081 Ulm, Germany

11. Université de Strasbourg, CNRS, INSERM, Institut de Génétique et de Biologie Moléculaire et Cellulaire - UMR 7104, Illkirch-Graffenstaden, France

Corresponding author email address:

thomas.bourgeron@pasteur.fr

ferhat.allainthibeault@gmail.com

Abstract

Autism spectrum disorders (ASD) are characterised by atypical social communication and stereotyped behaviours. Mutations in the gene encoding the synaptic scaffolding protein SHANK3 are detected in 1-2% of patients with ASD and intellectual disability (ID), but the mechanisms underpinning the symptoms remain largely unknown. Here, we characterized the behaviour of *Shank3* mutant mice deleted for exon 11 (*Shank3*$^{\Delta 11/\Delta 11}$) from three to twelve months of age. We observed decreased locomotor activity, increased stereotyped self-grooming and atypical socio-sexual interaction compared to wild-type littermates. We then used RNAseq on four brain regions of the same animals to identify differentially expressed genes (DEG). DEGs were identified mainly in the striatum and were associated with synaptic transmission (e.g. *Grm2, Dlgap1*), G-protein-signalling pathways (e.g. *Gnal, Prkcg1, and Camk2g*), as well as excitation/inhibition balance (e.g. *Gad2*). Downregulated and upregulated genes were respectively enriched in the gene clusters of medium-sized spiny neurons expressing the dopamine 1 (D1-MSN) and the dopamine 2 receptor (D2-MSN). Moreover, expression of DEGs reported as striosome markers within the striatum (*Cnr1, Gnal1, Gad2, and Drd4*) were positively correlated with excessive self-grooming. Finally, we showed that the striosome compartment of *Shank3*$^{\Delta 11/\Delta 11}$ mice was enlarged and displayed higher expression of GAD65 compared to wild-type mice. Altogether, these results shed light on a possible role of the striosomes/matrix imbalance in excessive self-grooming in *Shank3*$^{\Delta 11/\Delta 11}$ mice. Such striatal alterations could be present in a subgroup of patients with ASD and ID and could open the way to new therapeutic approaches.

Introduction

Autism spectrum disorders (ASD) are neurodevelopmental conditions characterised by atypical social communication and interactions associated with stereotyped behaviours and restricted interests (1). More than 200 genes have been robustly associated with ASD pointing at biological pathways such as chromatin remodelling and synaptic function (2). Among these genes, *SHANK3* (SH3 and multiple ankyrin repeat domain 3) codes for a scaffolding protein located at the postsynaptic density (PSD) of glutamatergic synapses where it interacts with other scaffolding proteins, cytoskeletal proteins, glutamate receptors and signalling molecules (3).

Heterozygous *de novo* mutations deleting the *SHANK3* gene on chromosome 22q13.3 or affecting its coding region are associated with Phelan-McDermid syndrome (4) and observed in 1-2% of patients with both ASD and intellectual disability (ID), making this gene a major cause of neurodevelopmental disorders (NDD) (5,6). Remarkably, a relatively high proportion of patients (>60%) carrying *SHANK3* mutations display regression (i.e., substantial loss of language and social skills) during adolescence and adulthood (7,8). However, the mechanisms of this worsening of the phenotype remain unknown.

Through the use of multiple intragenic promoters and alternative splicing, several SHANK3 protein isoforms are differentially expressed according to developmental stage or brain region (9). Numerous *Shank3* mutant mice have been generated [for reviews see (3,10)]. Most of them bear deletion of specific exons still allowing the expression of some minor isoforms (9,11). The behavioural deficits reported for *Shank3* mutant mice depend on the strains and experimental conditions. However, the presence of stereotyped-like behaviours, such as excessive self-grooming, was reported in all *Shank3* mutant mice and is reminiscent of the stereotyped behaviours observed in patients with ASD (3,12,13). Stereotyped behaviours are frequently associated with anomalies of the striatum (14), a region that coordinates multiple aspects of cognition, including action planning, decision-making, motivation, reinforcement, and reward perception as well as motor control. Several studies identified anomalies in the striatum of *Shank3* mutant mice at the anatomical (e.g., larger volume), circuit (e.g., disruption of indirect pathway of basal ganglia) and cellular (e.g., decreased striatal expression of GluN2B, a NMDA

receptor subunit) levels (15–20). The biological pathways underpinning the observed abnormalities as well as the biomarkers predictive of phenotypic severity remain however largely unknown.

In the present work, we first conducted a thorough longitudinal behavioural characterization of *Shank3*$^{\Delta 11/\Delta 11}$ mice, carrying a deletion of exon 11 of *Shank3* (which still allow the expression of minor protein isoforms) (21), at three, eight and twelve months of age, focusing on social interactions and stereotyped behaviours. We then compared gene expression in four brain structures - cortex, hippocampus, cerebellum and striatum - in *Shank3*$^{+/+}$ and *Shank3*$^{\Delta 11/\Delta 11}$ male littermates characterised in the behavioural study. Compared to the other brain regions, the striatum appeared to be highly sensitive to the loss of the major SHANK3 protein isoforms. We also identified a correlation between the level of self-grooming and an increased striatal expression of several genes, including *Gad2* encoding GAD65, which catalyses the transformation of glutamate into GABA. Finally, using immunofluorescence on the striatum sections at 12 months, we found that the expression of GAD65 is increased in the patch/striosome compartment of the *Shank3*$^{\Delta 11/\Delta 11}$ mice compared to wild-type littermates and that the surface of this compartment is also increased, relative to the matrix compartment. Our results suggest that signalling imbalance between the striosome and matrix compartments of the striatum causes excessive self-grooming in *Shank3*$^{\Delta 11/\Delta 11}$ mice.

Material & methods

Animals and cohorts

Shank3$^{\Delta 11/\Delta 11}$ mice were generated by Genoway (Lyon, FRANCE) using 129S1/SVImJ ES cells. The *Shank3* mutation, deletion of exon 11, was then transferred onto a C57BL/6J background with more than 15 backcrosses (21). In this model, short protein isoforms are still expressed (21). Food and water were provided *ad libitum*. The experimenters were blind to the genotype of the tested animals for data collection and analyses. We bred *Shank3*$^{\Delta 11/+}$ males and females to obtain *Shank3*$^{+/+}$, *Shank3*$^{+/\Delta 11}$ and *Shank3*$^{\Delta 11/\Delta 11}$ littermates. For behavioural tests, we used three cohorts (including both males and females) that we analysed separately. See **Supplementary Methods** for details on the cohorts.

Ethical statement

All procedures were validated by the ethical committee of the Institut Pasteur (CEEA n°89) and of the Sorbonne Université (CEEA n°5) and were conducted under the approval of the Ministère de l'Enseignement Supérieur, de la Recherche et de l'Innovation under the reference APAFIS#7706-20 161 12317252460 v2 and reference APAFIS#3234-2015121619347680 v7, respectively.

Behavioural tests

Dark/light test, Elevated Plus-maze test, locomotion and exploratory test in the open field, rotarod, occupant/new-comer social test with ultrasonic vocalisation recording, male behaviour in presence of an oestrous female, three-chambered social test and starmaze test were used to investigate the mice's behaviours. The protocols of these tests are detailed in the "behavioural tests" section of the **Supplementary Methods.**

Observation of stereotyped behaviour

Mice were individually placed in a new test cage (Plexiglas, 50 x 25 x 30 cm; 100 lux; clean sawdust bedding) in a soundproof chamber. After 10 min habituation, we recorded their behaviour for 10 min (camera Logitech C920). We manually scored the time spent self-grooming and digging (The Observer, Noldus Information Technology). When scoring self-grooming, we did not take into account the scratching behaviour. The total duration and the average duration of each behavioural category were calculated.

Behavioural statistics

All group data are represented as mean ± standard error of the mean (s.e.m.), as well as the individual points. All statistics were performed with R software (22). In all behavioural tests, *Shank3*$^{+/\Delta 11}$ mice were not significantly different from *Shank3*$^{+/+}$ unless otherwise specified (see **Table S1**). Given the limited sample size and the non-normality of the data, comparisons between genotypes were performed using non-parametric Mann-Whitney U-tests. We used the non-parametric Friedman test to examine the effect of age within each genotype. Between age points, post-hoc tests were performed using paired Wilcoxon signed-rank tests. To analyse the variability within groups, the variances of the raw data were compared using Ansari-Bradley tests. If required, a Bonferroni correction for multiple testing was performed. Differences between groups were considered significant when $p<0.05$.

Transcriptome analysis

Tissue collection, total RNA extraction and sequencing, mapping and reference genome, calling variants from the RNAseq data and differential expression analysis are detailed in the "Transcriptome analysis" section of the **Supplementary Methods.**

Gene set and protein-protein interaction network analysis

Gene set over-representation analyses were performed based on Ensemble of Gene Set Enrichment Analyses (EGSEA) without considering the genes around the *Shank3* gene. Protein-protein interaction (PPI) networks were generated using the DEGs for the four brain structures independently. A randomised protein interaction network was created using all DEGs to determine the probability of finding a network. Software, packages and databases are detailed in "Gene set and protein-protein interaction network analysis" section of the **Supplementary Methods.**

Quantitative RT-PCR (q-RT-PCR) and RNA and protein fluorescent detection on striatum sections

We selected several genes of interest by cross checking the DEGs, ORA (gene ontology – GO –, Kyoto encyclopaedia of genes and genomes – KEGG– and Pathway), and data from the literature. To validate these genes, we used q-RT-PCR, either with the droplet digital Polymerase Chain Reaction (dd-PCR) or with the real time quantitative PCR (q-PCR) technology. These procedures are detailed in the "Quantitative RT-PCR" section of the **Supplementary Methods.** All statistical analyses were performed using R software (22). The comparison between genotypes was performed using Mann-Whitney U-tests. Single-molecule Fluorescent In Situ Hybridization (smFISH) experiment to detect *Drd1* and *Drd2* RNAs and immunofluorescence experiment and image analysis to quantify GAD65 immunoreactivity in the dorsal striatum are detailed in the ""Single-molecule Fluorescent In Situ Hybridization and immunofluorescence experiments on brain sections" and "Quantitative analysis of GAD65 immunoreactivity" section of the **Supplementary Methods.**

Results

Hypoactivity, atypical social behaviour and excessive self-grooming in *Shank3*$^{\Delta 11/\Delta 11}$ mice

At three months of age, *Shank3*$^{\Delta 11/\Delta 11}$ mice displayed typical body weight, normal motor coordination, typical anxiety-like behaviour levels and intact working memory, compared to *Shank3*$^{+/+}$ littermates (**Fig. S1**). In the open field, *Shank3*$^{\Delta 11/\Delta 11}$ males travelled significantly shorter distances in comparison

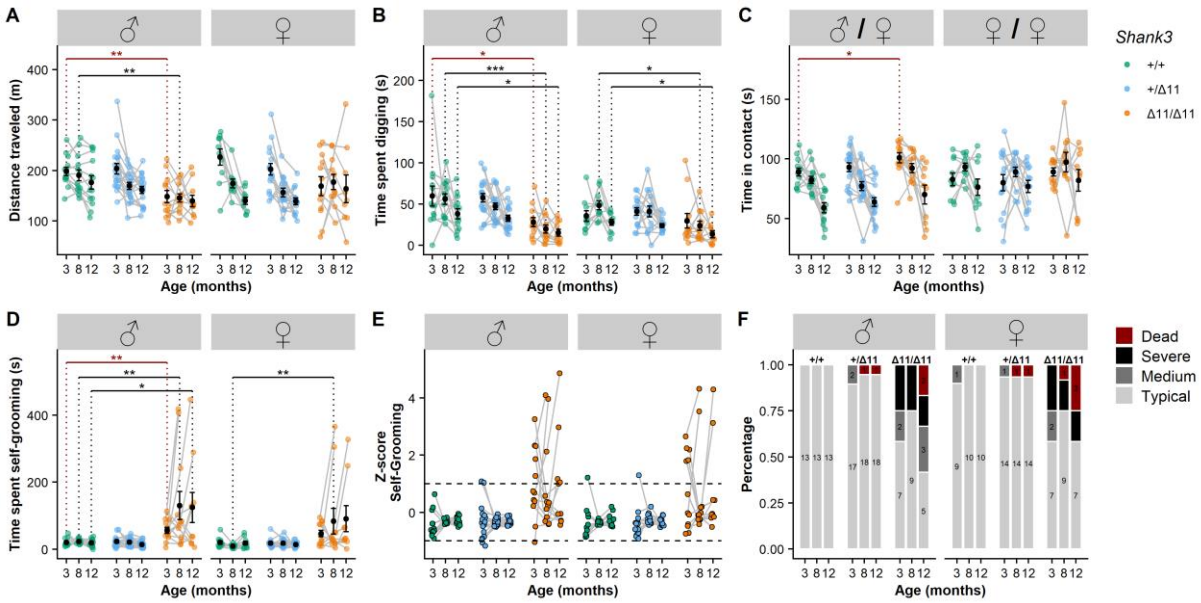

Figure 1: Hypoactivity, reduced exploration and increased stereotyped behaviours in *Shank3*$^{\Delta 11/\Delta 11}$ mice at three, eight and twelve months of age. (A) Total distance travelled during 30-min free exploration of an open field in wild-type (green), heterozygous (blue) and *Shank3*$^{\Delta 11/\Delta 11}$ (orange) for males (left panel) and females (right panel). (B) Total time spent digging in fresh bedding during 10 min observation in a new test cage, after 10 min habituation. (C) Total time spent in contact during male/female and female/female social interaction. (D) Total time spent self-grooming during 10 min observation in a new test cage, after 10 min habituation. (E) Z-score for the time spent self-grooming. (F) Number of individuals displaying different levels of severity in self-grooming. "Dead" corresponds to animals that had to be euthanized due to severe self-inflicted injuries. A-D: Black points represent mean with standard error of the mean (s.e.m). Mann–Whitney U test with Bonferroni correction for multiple testing (2 tests): *: corrected p-value <0.05; **: corrected p-value <0.01. Red lines represent statistics at 3 months of age; black lines represent statistics at 8 and 12 months of age.

with *Shank3*$^{+/+}$ littermates (Cohort 1: W=130, p=0.007; **Fig. 1A,** left panel; confirmed in Cohort 2 and Cohort 3: **Fig. S2**). *Shank3*$^{\Delta 11/\Delta 11}$ males also spent less time digging in the bedding in comparison with *Shank3*$^{+/+}$ mice (Cohort 1: W=123, p=0.027; **Fig. 1B;** Cohort 2: W=173, p<0.001; **Fig. S2**). A similar trend was present, but did not reach significance levels in females for activity and digging behaviour (Cohort 1: W=92, p=0.07; **Fig. 1A, B**). Remarkably, in stressful swimming conditions, *Shank3*$^{\Delta 11/\Delta 11}$ mice swam at a significantly higher speed compared to wild-type mice in the Morris water maze with visible platform (Cohort 3: p<0.01 over all training) and in the star maze (p<0.01), without any significant difference to find the direct path in the star maze (**Fig. S2**).

Impairments in social interactions and communication were not always observed in the different *Shank3* mouse models (10). Here, mice of all genotypes and both sexes displayed a typical preference for a same-sex conspecific in the three-chambered test (**Fig. S3**). No significant difference was observed in the latency for the first contact, in the total time spent in contact with same sex conspecific, in the

time spent in the different social behaviours and in the emission of the ultrasonic vocalizations (USVs) (**Fig. S3**). In contrast, we observed that *Shank3*$^{\Delta 11/\Delta 11}$ males spent significantly more time in contact with an oestrous female compared to *Shank3*$^{+/+}$ males (W=32, p=0.034; **Fig. 1C**), especially for oro-oral contact (W=22, p=0.005; **Fig. S3**). We also observed a reduction of time keeping the female in the visual field for *Shank3*$^{\Delta 11/\Delta 11}$ males compared to *Shank3*$^{+/+}$ males (W=133, p=0.006; **Fig. S3**). These altered behaviours were not accompanied with atypical vocal behaviour (**Fig. S3**).

At 3 months of age, *Shank3*$^{\Delta 11/\Delta 11}$ male mice already displayed a significant increase in the time spent self-grooming in comparison with *Shank3*$^{+/+}$ males (Cohort 1: W=21, p=0.002; Cohort 2: W=43, p=0.022). Similar trends did not reach significance in female mice (**Fig. 1, Fig. S2**). Interestingly, a higher group heterogeneity was observed in *Shank3*$^{\Delta 11/\Delta 11}$ mice in comparison with *Shank3*$^{+/+}$ mice (Cohort 1: males: Ansari Bradley test AB=111, p=0.036; females: AB=82, p=0.009; **Fig. 1D**). Furthermore, a subsample of *Shank3*$^{\Delta 11/\Delta 11}$ males (5 individuals over 12) and females (6 individuals over 12) presented hair removal that evolved into self-injuries.

Shank3 mutant mice display excessive self-grooming behaviour with age

Considering the frequent regression of patients carrying *SHANK3* mutations, we tested whether a phenotypic deterioration occurred in *Shank3*$^{\Delta 11/\Delta 11}$ mice. For that purpose, we tested exploratory activity, social communication and stereotyped behaviours in mice at eight and twelve months of age. The reduction of distance travelled in *Shank3*$^{\Delta 11/\Delta 11}$ mice compared to *Shank3*$^{+/+}$ mice was not present at older age; only *Shank3*$^{+/+}$ and *Shank3*$^{+/\Delta 11}$ mice reduced their activity with increasing age (**Fig. 1A**). Genotype-related differences in digging behaviour persisted with increasing age (8 months: W= 140, p<0.01; 12 months; W=107; p=0.01; **Fig. 1B**).

During social interactions, we observed a decrease of the time spent in contact over age, in particular for *Shank3*$^{+/+}$ males (Friedman test: F=7.384, p=0.025), *Shank3*$^{+/\Delta 11}$ males (F=12.316, p=0.002) and *Shank3*$^{+/+}$ females (F=7.400, p=0.025) and a tendency for *Shank3*$^{\Delta 11/\Delta 11}$ males without reaching significance **(Fig. 1C & S3)**. In female-female interactions, no behavioural differences between genotypes were observed at eight and twelve months of age, similarly to tests conducted at three months of age (**Fig. S3**). At eight months of age, the duration of oro-oral contact in *Shank3*$^{\Delta 11/\Delta 11}$ males

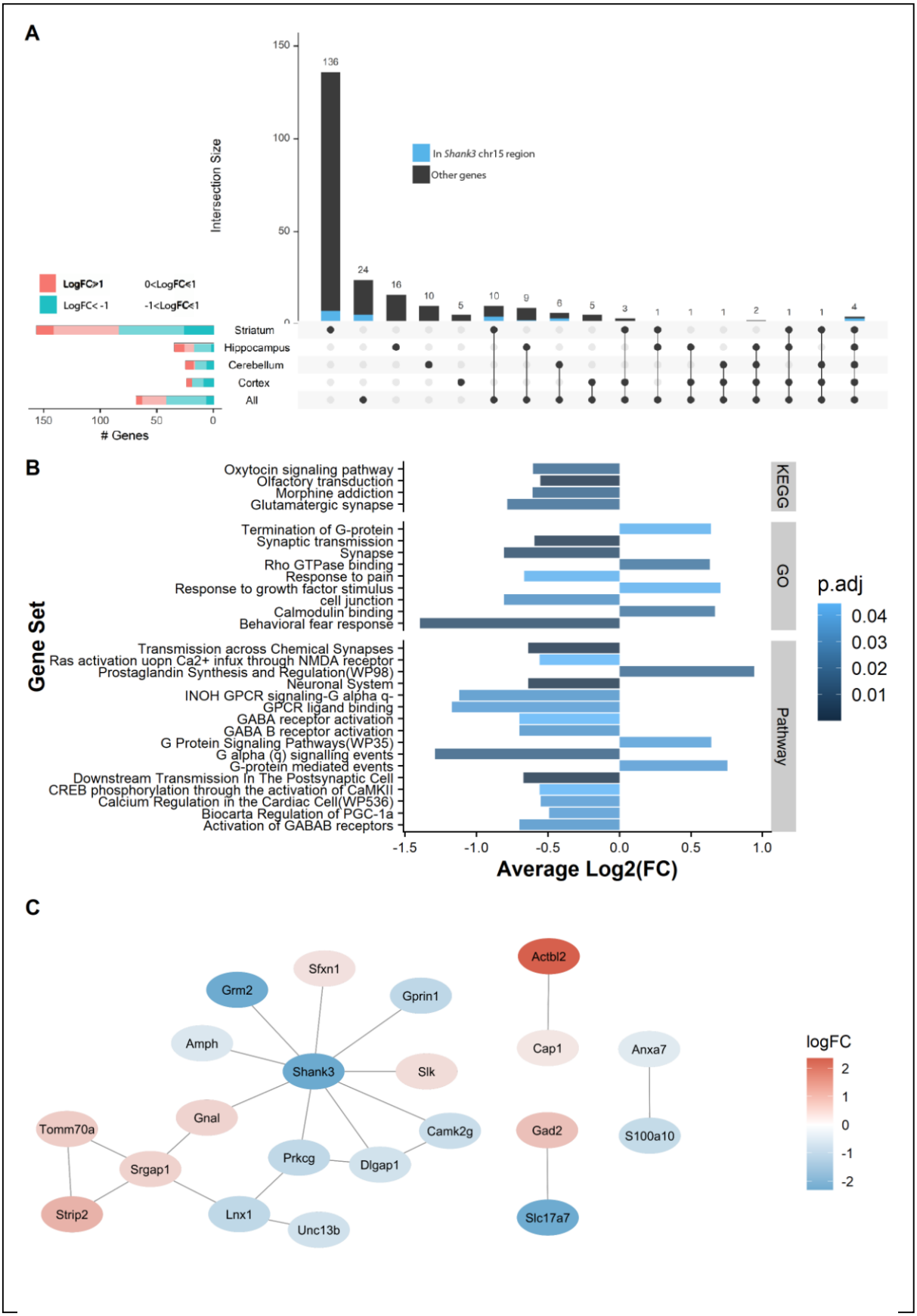
A
Intersection Size
In Shank3 chr15 region
Other genes
LogFC>1
0<LogFC<1
LogFC< -1
-1<LogFC<1
Striatum
Hippocampus
Cerebellum
Cortex
All
Genes
B
Gene Set
KEGG
GO
Pathway
Oxytocin signaling pathway
Olfactory transduction
Morphine addiction
Glutamatergic synapse
Termination of G-protein
Synaptic transmission
Synapse
Rho GTPase binding
Response to pain
Response to growth factor stimulus
cell junction
Calmodulin binding
Behavioral fear response
Transmission across Chemical Synapses
Ras activation uopn Ca2+ infux through NMDA receptor
Prostaglandin Synthesis and Regulation(WP98)
Neuronal System
INOH GPCR signaling-G alpha q-
GPCR ligand binding
GABA receptor activation
GABA B receptor activation
G Protein Signaling Pathways(WP35)
G alpha (q) signalling events
G-protein mediated events
Downstream Transmission In The Postsynaptic Cell
CREB phosphorylation through the activation of CaMKII
Calcium Regulation in the Cardiac Cell(WP536)
Biocarta Regulation of PGC-1a
Activation of GABAB receptors
p.adj
Average Log2(FC)
C
Sfxn1
Grm2
Gprin1
Amph
Shank3
Slk
Gnal
Tomm70a
Srgap1
Prkcg
Dlgap1
Camk2g
Strip2
Lnx1
Unc13b
Actbl2
Cap1
Anxa7
Gad2
S100a10
Slc17a7
logFC

← **Figure 2: The striatum displays the largest gene expression differences between *Shank3*$^{+/+}$ and *Shank3*$^{\Delta 11/\Delta 11}$ mice and the largest number of impacted pathways.** (A) Upset plot displaying the intersection between brain structures for the genes differentially expressed between *Shank3*$^{\Delta 11/\Delta 11}$ and *Shank3*$^{+/+}$ mice (adjusted p-value < 0.05; determined by limma-voom using observation quality weights). Genes located around the *Shank3* region on chromosome 15 are shown in blue. The horizontal bar plots on the left show the number of differentially expressed genes in the different brain structures according to the value of their log-fold changes (logFC). (B) GO (Gene Ontology), GeneSetDB Pathway (gsdbpath), and KEGG (Kyoto Encyclopaedia of Genes and Genomes) gene sets found to be over-represented (top 20 gene sets with adjusted p-value < 0.05) in the genes detected as differentially expressed in the striatum. (C) Protein-protein interaction (PPI) network for the differentially expressed genes (DEGs). Nodes, coloured ovals, represent DEGs; edges, black lines, represent direct protein-protein interactions (from BioGrid) between DEGs products. The colour of the node represents the Log2FC of DEGs: red means up-regulation and blue means down-regulation in *Shank3*$^{\Delta 11/\Delta 11}$ mice compared to wild-type mice.

with an oestrous female was still significantly increased, similarly to what we observed at three months (W=29, p=0.025), but these differences were no longer significant at twelve months of age (**Fig. S3**). Nevertheless, at this age, we detected an increase of the “approach then escape" behavioural sequence displayed by *Shank3*$^{\Delta 11/\Delta 11}$ males toward a C57BL/6J female in comparison with *Shank3*$^{+/+}$ males (W=15.5, p=0.005, **Fig. S3**).

At eight and twelve months of age, *Shank3*$^{\Delta 11/\Delta 11}$ males still displayed excessive self-grooming in comparison with *Shank3*$^{+/+}$ mice (eight months: W=27, p=0.009; twelve months: W=37, p=0.041; **Fig. 1D**). The same was true for *Shank3*$^{\Delta 11/\Delta 11}$ females who also groomed themselves significantly more than *Shank3*$^{+/+}$ females (eight months: W=11, p=0.002; twelve months: W=20, p=0.014; **Fig. 1C**). Interestingly, higher inter-individual variability was still present in *Shank3*$^{\Delta 11/\Delta 11}$ mice compared to *Shank3*$^{+/+}$ mice (at eight months for males: AB=118, p=0.002; and females: AB=75, p=0.044; at twelve months for males: AB=102, p<0.001; **Fig. 1E**). With age, an increasing number of *Shank3*$^{\Delta 11/\Delta 11}$ mice were outliers, performing self-grooming during a period exceeding two standard deviations (thresholds for males: 3 months: >80.8s; 8 months: >231s; 12 months: >208.4s; thresholds for females: 3 months: >78.3s; 8 months: >188.8s; 12 months: >171.8 s) or had to be euthanized because of severe self-inflicted injuries. Nevertheless, for 4 out of 12 *Shank3*$^{\Delta 11/\Delta 11}$ males and 3 out of 12 *Shank3*$^{\Delta 11/\Delta 11}$ females, we did not observe excessive self-grooming at any of the three time points (**Fig. 1E, F**).

Differential expression of genes related to synaptic function, signalling and cytoskeleton dynamics in the striatum of *Shank3*$^{\Delta 11/\Delta 11}$ mice

To investigate the impact of the loss of the major SHANK3 isoforms on the transcriptome, we performed RNAseq on four brain structures (whole cortex, striatum, hippocampus, and cerebellum) of seven *Shank3*$^{+/+}$ and eight *Shank3*$^{\Delta 11/\Delta 11}$ male mice after their behavioural characterization at twelve months of age. DEGs between *Shank3*$^{+/+}$ and *Shank3*$^{\Delta 11/\Delta 11}$ mice (FDR < 0.05) across and within structures (**Table S2**) were enriched in genes located in the vicinity of the *Shank3* locus on chromosome 15, most likely due to the residual genomic region from the 129S1/SvImJ ES cells used to generate the *Shank3*$^{\Delta 11/\Delta 11}$ mice (**Fig. S4**) (21). We therefore excluded these genes from the analyses (more details in **Supplementary methods**). We also performed quantitative RT-PCR (q-RT-PCR) to confirm up- or downregulation of 30 DEGs (Spearman correlation R=0.809 P<0.0001; **Supplementary Fig. S5**). As expected, *Shank3* expression levels in all four brain structures were significantly reduced in *Shank3*$^{\Delta 11/\Delta 11}$ mice in comparison with *Shank3*$^{+/+}$ mice (FDR < 0.001; **Fig. S6**). Notably, the *Shank3* sequence reads still present in the *Shank3*$^{\Delta 11/\Delta 11}$ mice were aligned to exons downstream of exon 11 (**Table S2**). No significant changes in the expression of *Shank1* and *Shank2* were found (**Fig. S6**, **Table S2**).

We examined the DEGs (FDR < 0.05) within each of the four brain structures. The largest number of DEGs was detected for the striatum with 140 DEGs. The hippocampus displayed 26 DEGs, the cortex 13 and the cerebellum 16 (**Fig. 2A**). After removing the genes and pseudogenes located around the *Shank3* locus, *Shank3* was the only gene differentially expressed in the four brain structures (**Fig. 2A**). The DEGs in the striatum displayed an increased dispersion compared to the other structures, indicating an increased variability of response between animals (**Fig.S7**). Altogether, these results suggest that, among the four structures studied, the transcriptome of the striatum is by far the most impacted by the loss of the major isoforms of SHANK3.

We investigated the functions of the proteins encoded by the DEGs in the striatum using over-representation analysis (ORA) and Protein-Protein Interaction (PPI) analysis. The ORA (**Table S3**) revealed enrichment in DEGs associated with, among others, two pathways of interest: synaptic transmission (negative fold-change in *Shank3*$^{\Delta 11/\Delta 11}$ mice in comparison with *Shank3*$^{+/+}$ mice), and G-

protein activity (positive and negative fold-change in *Shank3*$^{\Delta 11/\Delta 11}$ mice in comparison with *Shank3*$^{+/+}$ mice according to the type of G-protein pathway) (**Fig. 2b** and **Table S3**). PPI analysis of the striatal DEGs highlighted one network of 15 proteins (p-value from randomized network: <0.01; **Fig. 2C**), some of them directly interacting with SHANK3 in the PSD, such as the metabotropic glutamate receptor 2 (encoded by *Grm2*, highly decreased) and Disks large-associated protein 1, a scaffolding protein (encoded by *Dlgap1*, also decreased) interacting with AMPA and NMDA receptors. In addition to these synaptic proteins, the network contains proteins involved in signal transduction (e.g. *Prkcg1*, *Camk2g*) and cytoskeleton dynamics (e.g. *Slk*). Other small networks identified by the PPI analysis contain proteins involved in glutamate transportation (*Slc17a7*) and decarboxylation (*Gad2*), and cytoskeleton dynamics (*Actbl2*).

<u>Cellular expression pattern of the DEGs expressed in the striatum of *Shank3*$^{\Delta 11/\Delta 11}$ mice</u>

The inhibitory medium-sized spiny neurons (MSN) constitute the major type of striatal neuronal population. They receive glutamatergic inputs and are the target of dopamine innervation from cortex, thalamus, amygdala and substantia nigra pars compacta (SNpc) (23). Most of these MSN express either dopamine 1 receptor DRD1 (D1-MSN, belonging to the direct pathway), dopamine 2 receptor DRD2 (D2-MSN, belonging to the indirect pathway), or both receptors for a small fraction of MSN. In order to identify the striatal cell types which are the most impacted by SHANK3 deficiency, we compared the expression pattern of the DEGs with marker genes of striatal cell types reported in two single-cell RNA sequencing studies (24,25). We observed that DEGs under-expressed in *Shank3*$^{\Delta 11/\Delta 11}$ compared to *Shank3*$^{+/+}$ mice were enriched in the D1-MSN clusters while overexpressed genes were enriched in the D2-MSN clusters (**Fig. 3A, Table S2 & S4**). This could reflect a modified proportion of D1-MSN (decrease) and D2-MSN (increase) in the striatum of the *Shank3*$^{\Delta 11/\Delta 11}$ mice. However, many genes commonly considered as specific to D1-MSN (*Drd1*, *Isl1*, *Sfxn1* and *Tac1*) or D2-MSN (*Drd2*, *Adora2a*, *Penk*, *Gpr6*, *Sp9*) were not found to be differentially expressed in the *Shank3*$^{\Delta 11/\Delta 11}$ animals (**Table S2**). Moreover, using Single Molecule RNA Fluorescence In Situ Hybridization with *Drd1* and *Drd2* RNA probes, we observed no significant difference in the number of D1 and D2 striatal neurons between the *Shank3*$^{\Delta 11/\Delta 11}$ and *Shank3*$^{+/+}$ mice (**Fig. S8**). Altogether, these results indicate that the deletion of exon

289

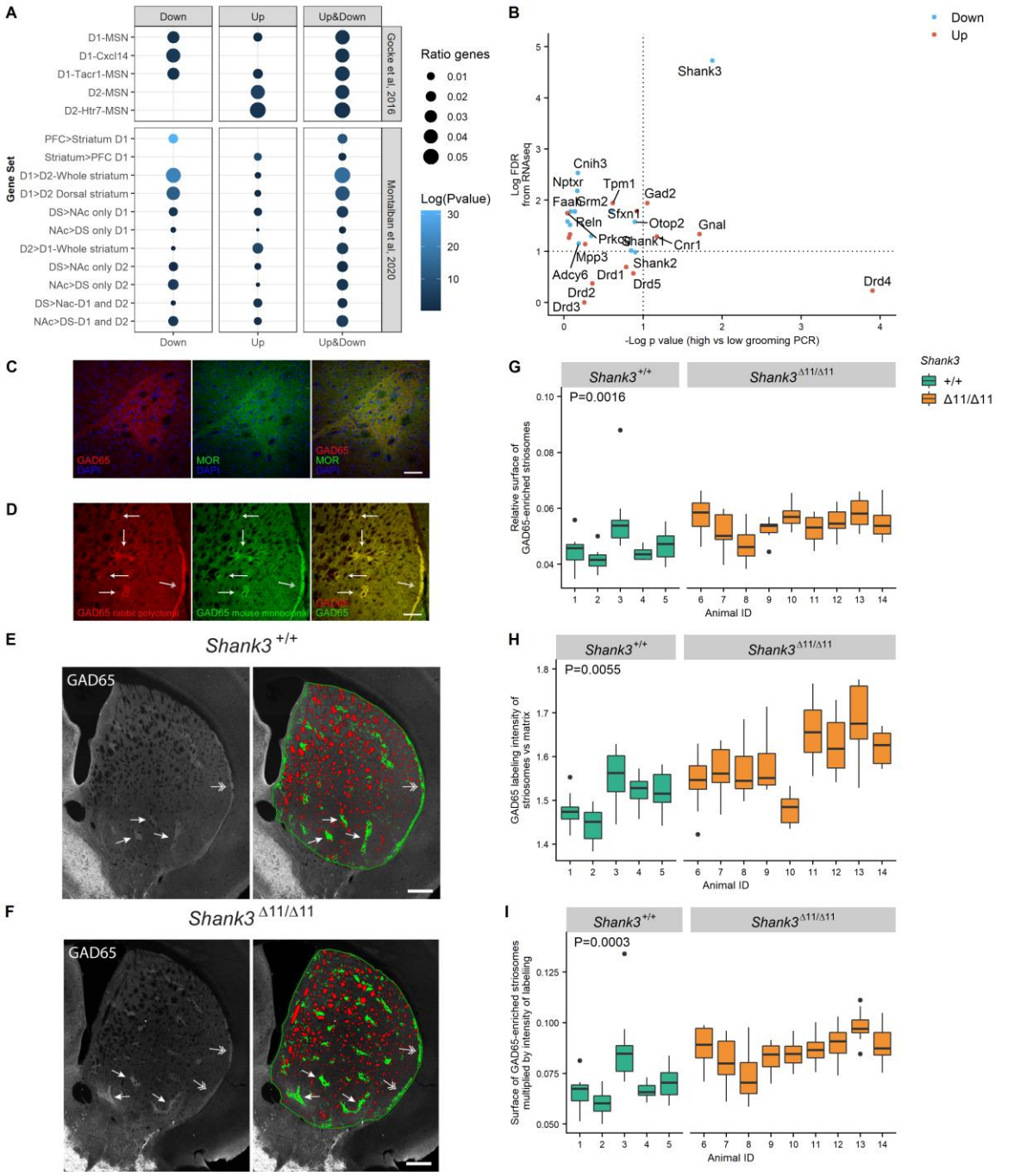

Figure 3: Altered transcriptome of D1- and D2-MSN and higher expression of GAD65 in the striosomal compartment in the striatum of *Shank3*$^{\Delta11/\Delta11}$ mice.

(A) Enrichment of RNAseq DEGs in the striatum of *Shank3*$^{\Delta11/\Delta11}$ mice compared to cell-specific gene clusters suggested by Gokce et al. (2016) and Montalban et al. (2020). Genes under-expressed in *Shank3*$^{\Delta11/\Delta11}$ striatum are enriched in D1-MSN clusters while genes over-expressed in *Shank3*$^{\Delta11/\Delta11}$ striatum are enriched in D2-MSN clusters. Ratio genes correspond to the proportion of DEGs enriched into the cluster. Over-representation analyses were performed with Fisher's hypergeometric tests and p-values were adjusted for multiple testing with the Benjamini-Hochberg procedure within each category of DEGs. (B) Comparison of the log of p-values for the differential expression of selected genes in *Shank3*$^{+/+}$ vs *Shank3*$^{\Delta11/\Delta11}$ mice and the log of p-values for low self-grooming vs high self-grooming. (C-D) Confocal images of striatum coronal sections of one-year old *Shank3*$^{+/+}$ male mice. (C) GAD65 immunoreactivity (red) is enriched in striatal microzones identified as striosomes by immunostaining for μ-opioid receptor (MOR, in green), a canonical marker of striosomes. (D) Increased GAD65 immunoreactivity in striosomes (arrows) and subcallosal streak (two-headed arrows)

← compared to surrounding matrix is observed with two different antibodies:the rabbit polyclonal antibody (Invitrogen PA5-77983 in red) used in C, E, F and a mouse monoclonal antibody (Millipore MAB351, in green). (E-F) Distribution and quantification of GAD65 immunoreactivity in dorsal striatum sections of a *Shank3*$^{+/+}$ (E) and a *Shank3*$^{\Delta 11/\Delta 11}$ (F) mouse. The arrows point to striosomes and the arrowheads to subcallosal streak. The unlabelled myelinated fibres are coloured in red. The regions of higher expression of GAD65 (striosomes) are coloured in green, and the regions of lower expression of GAD65 (matrix) are uncoloured. (G, H, I) Comparison of GAD65 immunoreactivity in the striosome and matrix compartments of the dorsal striatum in 5 *Shank3*$^{+/+}$ (green) and 9 *Shank3*$^{\Delta 11/\Delta 11}$ (orange) one-year old male mice. (G) Relative surface of the GAD65-enriched striosome compartment (surface of striosomes / surface of (striosomes + matrix). (H) Relative GAD65 labelling intensity in the striosome compartment compared to the matrix compartment (GAD65 labelling in striosomes / GAD65 labelling in matrix). (I) Overall GAD65 immunoreactivity in the striosomal compartment (relative surface (G) multiplied by the relative GAD65 labelling intensity (H)). Data, generated from analysis of 9 to 14 images per animal, are presented as box-plots (median, first, and third quartiles). Scale bars: 50 µm (C), 200 µm (D), 500 µm (E, F).

11 of *Shank3* leads to differential transcriptional alterations in the D1- and D2-MSN, without major difference in the number of these types of neurons throughout the whole striatum.

<u>Genes with expression that correlate with excessive self-grooming</u>

Using RT-PCR, we investigated the correlation between the mRNA level in the striatum of DEGs identified by RNAseq analysis and other genes of interest (*Shank1*, *Shank2, and Drds*) and the level of self-grooming observed in seven 12 months-old *Shank3*$^{\Delta 11/\Delta 11}$ mice. We found that excessive grooming was associated with higher levels of transcripts for four of the DEGs identified by RNAseq or RT-PCR: *Cnr1*, *Gnal*, *Gad2*, and *Drd4* (**Fig. 3B; FigS9**). *Cnr1* encodes the cannabinoid receptor 1; *Gnal* encodes a stimulatory G-alpha subunit of a heterotrimeric G-protein (Gαolf); *Gad2* codes for GAD65, one of the two enzymes that convert glutamate into γ-aminobutyric acid (GABA), and *Drd4* encodes the dopamine receptor 4. Interestingly, these proteins have been reported to be heterogeneously distributed in the dorsal striatum, being more abundant in the spatial microzones known as striosomes or patches than in the much larger matrix surrounding them (26–29). Given the function of GAD65, i.e. converting glutamate into GABA, an inhibitory transmitter, we studied its striatal distribution in the dorsal striatum, using immunofluorescence on brain sections (**Fig. 3C-I**). We found that GAD65 is enriched in striosomes, identified by co-labelling of µ-opioid receptor (MOR), the most widely used marker for striosomes of the rostral striatum (30) (**Fig. 3C**). GAD65 can thus be considered as a marker of the striosome compartment in mice. We also confirmed the specificity of GAD65 labelling using a second

independent GAD65 antibody (**Fig. 3D**). Both the relative surface occupied by the GAD65-enriched striosomes in the dorsal striatum and the GAD65 labelling intensity of these patches relative to matrix were increased in the *Shank3*$^{\Delta 11/\Delta 11}$ mice compared to the *Shank3*$^{+/+}$ mice (p = 0.0016 and p = 0.0055 respectively) (**Fig. 3E-H)**), leading to an increased GAD65 immunoreactivity in the striosome compartment vs the matrix compartment in *Shank3*$^{\Delta 11/\Delta 11}$ animals (p=0.0003, **Fig. 3I**).

Discussion

The present study highlighted robust behavioural deficits in *Shank3*$^{\Delta 11/\Delta 11}$ mutant mice, more specifically a reduced activity in the open field, atypical social behaviour in males interacting with oestrous females, and increased self-grooming compared to wild-type littermates. Interestingly, the majority of *Shank3*$^{\Delta 11/\Delta 11}$ mutant mice displayed excessive self-grooming, with a tendency to a worsening of the phenotype with increasing age for mice showing an early emergence of excessive grooming. At 12 months of age, the striatum had the most impacted transcriptomic profile compared to other brain regions. Further molecular characterizations suggest that the excessive self-grooming phenotype might be related to signalling imbalances between the striosome and the matrix compartments in the dorsal striatum.

Behavioural profiling of the Shank3*$^{\Delta 11/\Delta 11}$ *mutant mice

Atypical social interaction: Results from the literature have highlighted either reduced duration of social contact and reduced number of USVs emitted [e.g., *Shank3b* (31); *Shank3*$^{\Delta ex4\text{-}22}$ (32)] or no significant difference in socio-sexual behaviours [e.g., *Shank3*^{Q321R} (33)]. Here, we observed limited difference in social interaction with an increase in the time spent in contact for *Shank3*$^{\Delta 11/\Delta 11}$ males interacting with an oestrous female (observed at 3 and 8 months of age), and more specifically in nose-to-nose contacts, as already highlighted in previous studies [*Shank3*$\Delta^{ex14-16}$cKO (33); *Shank3*$^{\Delta 11/\Delta 11}$ females (34)]. Testing the specificity of this type of contact would help to understand its significance in mouse social communication. Further experiments should be designed to test whether this specific behaviour is associated with a deficit in social reward processing [as suggested for *Shank2*$^{\Delta 6\text{-}7/\Delta 6\text{-}7}$ mice (35)]. Indeed,

several studies have shown that SHANK3 controls maturation of social circuits in the ventral tegmental area (VTA) (36,37) and synaptic strength of D2-MSN in the striatum (16,20).

Excessive grooming: Excessive self-grooming has been observed in the majority of *Shank3* mutant mice over their lifetime and therefore represents the most robust behavioural phenotype in all models. Extreme self-grooming is not due to increased skin sensitivity since previous studies reported that rescuing normal tactile reactivity in *Shank3b*$^{+/-}$ does not improve over-grooming behaviour (38). In our study, we also observed an important inter-individual variability in this trait with 30% of the mutant mice that did not seem to display excessive grooming even after one year. Increased self-grooming might reflect a response to stressful conditions, which might vary from one individual to another (difference in susceptibility and/or exposure to stressful conditions). Such increased reactivity to stressful conditions is reminiscent of what is observed in patients and deserves further systematic testing in the different *Shank3* mutant models (39).

From transcriptome to imbalance of striatum compartments and excessive grooming

Abnormal striatal transcriptome: The massive impact of the *Shank3* mutation on the transcriptome profile of the striatum suggests that this region could be the centrepiece of the behavioural deficits observed in *Shank3* mutant mice. Several studies have already reported functional alterations of the striatum and more specifically of the MSN in the diverse *Shank3* mutant strains (12,15,16,20,36,37). Our report of an alteration of the striatal transcriptome could be due to a direct role of the SHANK3 protein through gene transcription. Indeed, previous studies have reported the presence of SHANK3 in the nucleus, especially the isoform SHANK3b, which is disrupted in our model. Alternatively, the abnormal striatal transcriptome profile could be the consequence of the alteration of the glutamatergic synapses that interfere with signal transduction, such as G protein (40) and mTOR (41) signalling, and then with gene transcription or mRNA stability. We found that several transcripts encoding proteins involved in glutamatergic synaptic transmission were under-expressed in *Shank3*$^{\Delta 11/\Delta 11}$ mice. For example, we observed a decrease of *Grm2*, encoding mGluR2, a G-protein-coupled glutamate receptor which interacts with the proline-rich domain of SHANK3 and which has been found decreased in a

valproate-induced rat model of autism (42). We also observed significant under-expression of *Dlgap1*, coding for DAP1/GKAP. This protein connects SHANK3 to the scaffolding protein PSD-95 (43) which recruits AMPAR and NMDAR. In contrast, we did not observe diminution of transcript levels for several proteins (GluA, GluN or mGluR5) previously shown as decreased in the synaptosomes or PSD fractions of *Shank3* mutant mice compared to wild type. A possible explanation is that the absence of SHANK3 decreases the translation or the recruitment of these proteins at the synapse or increases their degradation without affecting gene transcription and mRNA degradation.

A link between abnormal gene transcription, striatum organisation and excessive grooming: We observed that expression of *Gad2*, *Cnr1*, *Gnal* and *Drd4* was positively correlated with excessive self-grooming. Remarkably, three of these genes have been previously associated with self-grooming, but not always in the same direction. In contrast to our study, *Cnr1* deletions (as well as CB1R antagonists) have been reported to increase self-grooming behaviour (44–47). The overexpression of *Cnr1* in *Shank3*$^{\Delta 11/\Delta 11}$ mice might therefore result from a compensatory upregulation in response to the alterations of the endocannabinoid system which has been previously reported in SHANK3-deficient mice (20,48), in valproic acid induced rat models of ASD and also in some individuals with ASD (49). Consistent with our findings, *Gnal* haploinsufficiency is associated with a reduction of self-grooming behaviour in a mouse model of dystonia (50). Links between *Shank3* and *Gad2* were previously reported with an increase of GAD65 immunoreactivity in the *Shank3*ß$^{-/-}$ *mice* (44) and a decrease of *Gad2* transcript in the striatum of a *Shank3*-overexpressing model (51). To our knowledge, there is no direct evidence in the literature for an association between *Drd4* expression and grooming behaviour. It would thus be interesting in future studies to investigate this potential link.

Interestingly, these four genes have also been reported to be enriched in striosomes (26–29). These microzones of the dorsal striatum contain early born MSN and are embedded into the much larger surrounding matrix including late-born MSN (52). The two compartments, initially distinguished by differential expression of numerous molecular markers [for a review see (53)], also differ in their input and output connectivity and electrophysiological characteristics (54), such as D1-MSN excitability (55), rates of dopamine release (56), and response to chronic stress (57). Signalling imbalances between the

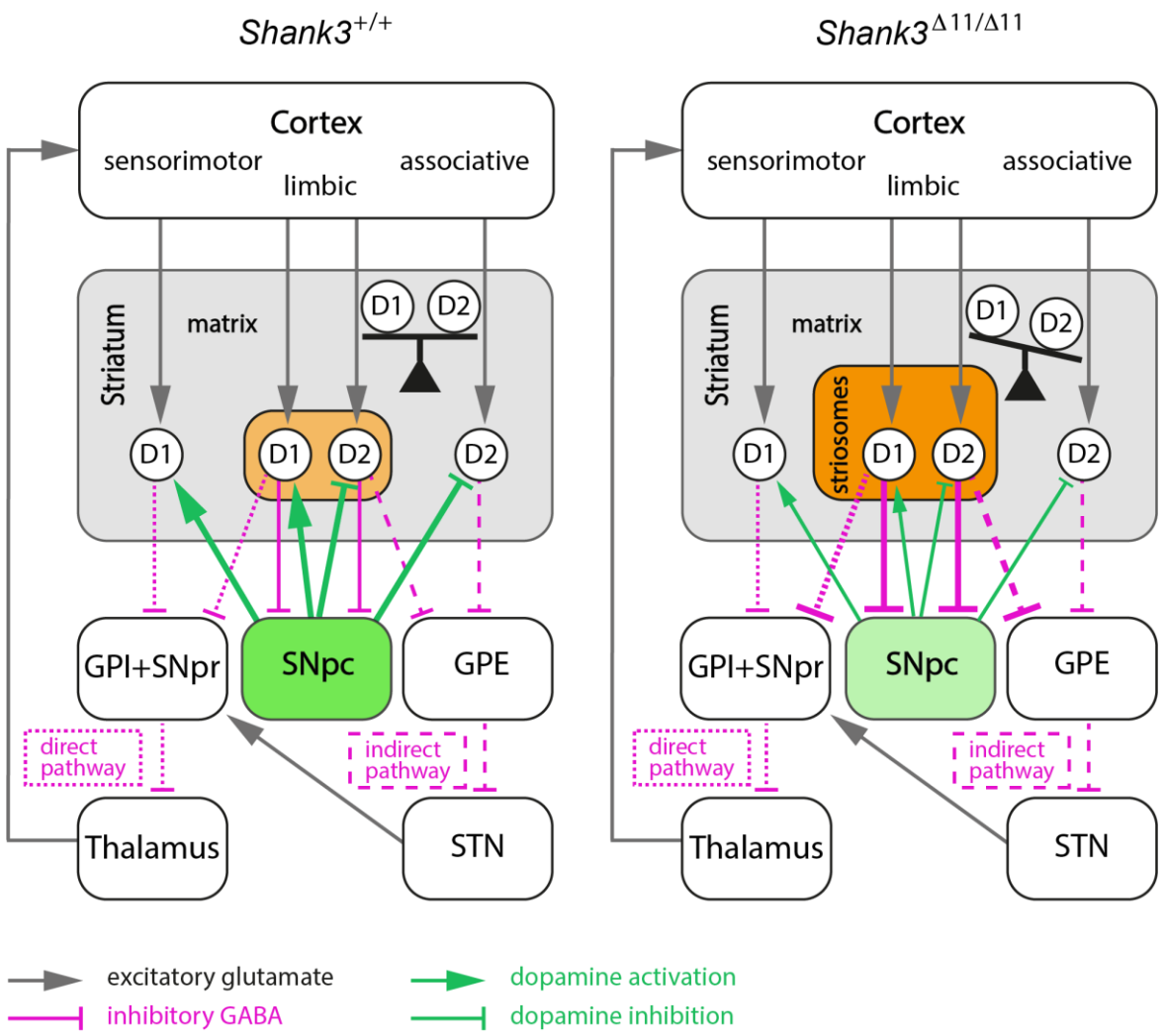

Figure 4: Proposed model linking increased activity in the striosomal pathway and imbalance between the direct and indirect pathways in the *Shank3*$^{\Delta 11/\Delta 11}$ mice. Increased activity of the striosomal pathway in *Shank3*$^{\Delta 11/\Delta 11}$ mice, due to both larger size and increased GAD65 activity of the striosomal compartment (light/dark orange) enhances GABAergic inhibition of the dopamine-producing neurons of SNpc (green). This inhibition of the SNpc neurons (light green) results in an imbalance between the direct and indirect pathways by decreasing both the activation of D1-MSN (D1) and the inhibition of D2-MSN (D2). GPI, internal globus pallidus; GPE, external globus pallidus; SNpr, substantia nigra pars reticulata; SNpc, substantia nigra pars compacta; STN, subthalamic nucleus.

striosome and matrix compartments have been implicated in several movement disorders [Huntington's disease, Parkinson's disease, dyskinesia, dystonia, for a review see (53)], psychostimulant-induced motor stereotypies (58,59), and more recently in anxiety disorders (60). Corticostriatal path targeting striosomes also control decision-making under cost-benefit conflict (61,62) and habit formation (63). Our finding that four striosome markers had increased expression associated with excessive self-grooming in *Shank3*$^{\Delta 11/\Delta 11}$ mice, prompted us to explore the compartmental architecture of the striatum in these mice. This investigation was also motivated by previous studies that have shown that enhanced

striosomal activation is highly correlated with increased repetitive behaviours, including self-grooming in both non-human primates and rodents [for review see (14)]. Moreover, studies by Kuo and Liu (64,65) have recently suggested that aberrant striatal compartmentation may be involved in ASD.

We first confirmed that GAD65, which had been reported to be a striosome marker in primates, but not in rats (27) was indeed a striosome marker in the mouse. We then found that both the surface and GAD65 labelling intensity of the striosome compartment relative to the matrix one are increased in *Shank3*$^{\Delta 11/\Delta 11}$ mice compared to *Shank3*$^{+/+}$ mice. Whereas the majority of GABA in brain is produced by the cytosolic isoform of glutamate decarboxylase (GAD67, encoded by *Gad1*), GAD65, which is anchored to the membrane of synaptic vesicles, can supply GABA in situations of high demand (66,67), such as stress or fear, and for fine tuning of inhibitory transmission. It is thus possible that an alteration of striosomes in *Shank3*$^{\Delta 11/\Delta 11}$ mice is responsible for excessive self-grooming observed in these mice.

A model for striosome/matrix imbalance as a possible cause of excessive grooming in the Shank3 mutant mice: It is well established that the striatum and the dopamine-containing nigrostriatal tract control self-grooming behaviour (14), and striosomal MSN are the predominant striatal population innervating dopamine neurons of the nigrostriatal tract (68). An imbalance between the striosome and the matrix compartments may then explain, via a modification of dopamine signalling, the excessive grooming of *Shank3*$^{\Delta 11/\Delta 11}$ mice (**Fig. 4**). Indeed, in contrast to MSN located in the matrix of the striatum, striosomal MSN projects directly to the dopamine-producing neurons in the SNpc (53,69). Then, SNpc dopamine neurons project back to the entire dorsal striatum. An increased activity of GAD65 in the striosomes, in a situation of stress for example, would lead to an inhibition of dopamine release by the SNpc and thus to a reduced dopamine modulation of both the direct and indirect pathways in the dorsal striatum. Because dopamine activation has opposite effects on D1- and D2-MSNs by increasing and decreasing cell excitability, respectively - a decreased dopamine release by SNpc is expected to result in diminishing D1-MSN activity and boosting MSN-D2 activity. The differential enrichment in up- and down-regulated DEGs in D2-MSN and D1-MSN could be related to previous observation of a distinct impairment of LTD in D2-MSNs, but not in D1-MSN (20) in *Shank3* mutant mice. Importantly, since striosome cells are generated before matrix cells during development (52) and SHANK3 seems to be

involved in the early stages of neuronal development (15,70,71), the enlargement of the total relative surface of striosomes observed in *Shank3*$^{\Delta 11/\Delta 11}$ mice may be due to a default in the compartmentation of the striatum during early development.

Conclusions and perspectives

Altogether, the present study precisely describes the effects over time of the *Shank3*$^{\Delta 11}$ mutation on mouse social and repetitive behaviours and suggests a critical role of the striatum in excessive self-grooming, probably through imbalances in two intertwined systems, the striosome/matrix compartments and the direct/indirect pathways. Although still preliminary, our results suggest that SHANK3 deficiency and, more generally, ASD could integrate the growing list of neurological conditions implicating an imbalance in the striosome/matrix compartmentation of the dorsal striatum. Future studies are necessary to understand the mechanisms at the origin of the striosome/matrix imbalance and consider the possibility of its reversibility.

Conflict of interest statement

The authors have declared that no competing interests exist.

Detailed author contributions:

ATF, ABi, EV, EE and TB conceived the experiments. ATF and EE designed and acquired behavioural data from cohorts 1 and 2. ATF extracted and dissected brains, extracted RNA from cohorts 1 and 2. ATF and FM designed and ATF acquired data from smFISH. ATF performed analysis and statistics of behaviour, PPI and smFISH. ABo, BFi and JFD performed the RNA sequencing. ABi and ATF performed the analyses of ORA. ATF, BFo and AL performed and analysed the results of quantitative RT-PCR. EV performed the immunofluorescence experiments, with the help of SC for brain collection. FdC performed quantitative image analysis. SC and AMLS genotyped the mice. JS, CR and LRR conducted the experiments on cohort 3. TMB generated the mouse model. ATF, ABi, EV, BF, FdC, EE and TB wrote the manuscript.

Acknowledgments

The authors thank the members of the Génétique Humaine et Fonctions Cognitives lab for helpful discussions, especially Jean-Pierre Bourgeois for his advice and expertise, Thomas Rolland for his assistance with data analysis and Nathalie Lemière for her assistance with sample collection. The authors thank Jean-Antoine Girault, Véronique Brault, and Sonia Garel for their advice and expertise. This research was supported by Institut Pasteur, the Bettencourt-Schueller Foundation, CNRS, Université de Paris, the Conny-Maeva Charitable Foundation, the Cognacq Jay Foundation, the Fondation de France, the Fondation pour la Recherche Médicale (FRM), the GIS "Autisme et Troubles du Neuro-Développement", the Roger de Spoelberch Foundation, the Eranet-Neuron (ALTRUISM) project, the Laboratory of Excellence GENMED (Medical Genomics) (grant no. ANR-10-LABX-0013 managed by the National Research Agency (ANR) part of the Investment for the Future program), the BioPsy Labex (ANR-10-LABX-BioPsy, ANR-11-IDEX-0004-02), AIMS-2-TRIALS which received support from the Innovative Medicines Initiative 2 Joint Undertaking under grant agreement No 777394 and the Inception program (Investissement d'Avenir grant ANR-16-CONV-0005). We gratefully acknowledge the UtechS Photonic Bioimaging (Imagopole), C2RT, Institut Pasteur, supported by the French National Research Agency (France BioImaging; ANR-10-INSB-04; Investments for the future). The views expressed here are the responsibility of the author(s) only. The EU Commission takes no responsibility for any use made of the information set out.

Bibliography

1. Association American Psychiatric. Diagnostic and Statistical Manual of Mental Disorders [Internet]. American Psychiatric Association; 2013. Available from: http://psychiatryonline.org/doi/book/10.1176/appi.books.9780890425596 https://psychiatryonline.org/doi/book/10.1176/appi.books.9780890425596

2. Leblond CS, Le T-L, Malesys S, Cliquet F, Tabet A-C, Delorme R, et al. Operative list of genes associated with autism and neurodevelopmental disorders based on database review. Mol Cell Neurosci. 2021 Jun;113:103623.

3. Monteiro P, Feng G. SHANK proteins: Roles at the synapse and in autism spectrum disorder. Nat Rev Neurosci. 2017 Mar;18(3):147–57.

4. Phelan K, McDermid HE. The 22q13.3 deletion syndrome (Phelan-McDermid syndrome). Mol Syndromol. 2012;2(3–5):186–201.

5. Durand CM, Betancur C, Boeckers TM, Bockmann J, Chaste P, Fauchereau F, et al. Mutations in the gene encoding the synaptic scaffolding protein SHANK3 are associated with autism spectrum disorders. Nat Genet. 2007 Jan;39(1):25–7.

6. Leblond CS, Nava C, Polge A, Gauthier J, Huguet G, Lumbroso S, et al. Meta-analysis of SHANK Mutations in Autism Spectrum Disorders: A Gradient of Severity in Cognitive Impairments. PLoS Genet. 2014;10(9).

7. Kohlenberg TM, Trelles MP, McLarney B, Betancur C, Thurm A, Kolevzon A. Psychiatric illness and regression in individuals with Phelan-McDermid syndrome. J Neurodev Disord [Internet]. 2020 Feb;12(1). Available from: https://pubmed.ncbi.nlm.nih.gov/32050889/

8. Rubeis SD, Siper PM, Durkin A, Weissman J, Muratet F, Halpern D, et al. Delineation of the genetic and clinical spectrum of Phelan-McDermid syndrome caused by SHANK3 point mutations. Mol Autism. 2018 Dec;9(1):31.

9. Wang X, Xu Q, Bey AL, Lee Y, Jiang YH. Transcriptional and functional complexity of Shank3 provides a molecular framework to understand the phenotypic heterogeneity of SHANK3 causing autism and Shank3 mutant mice. Mol Autism. 2014;5(1):30.

10. Ferhat A-T, Halbedl S, Schmeisser MJ, Kas MJ, Bourgeron T, Ey E. Behavioural Phenotypes and Neural Circuit Dysfunctions in Mouse Models of Autism Spectrum Disorder. Adv Anat Embryol Cell Biol. 2017;224:85–101.

11. Drapeau E, Riad M, Kajiwara Y, Buxbaum JD. Behavioral Phenotyping of an Improved Mouse Model of Phelan–McDermid Syndrome with a Complete Deletion of the Shank3 Gene. bioRxiv. 2018 Jan;5(3):ENEURO.0046-18.2018.

12. Peça J, Feliciano C, Ting JT, Wang W, Wells MF, Venkatraman TN, et al. Shank3 mutant mice display autistic-like behaviours and striatal dysfunction. Nature. 2011 Apr;472(7344):437–42.

13. Wang X, McCoy PA, Rodriguiz RM, Pan Y, Je HS, Roberts AC, et al. Synaptic dysfunction and abnormal behaviors in mice lacking major isoforms of Shank3. Hum Mol Genet. 2011 Aug;20(15):3093–108.

14. Kalueff AV, Stewart AM, Song C, Berridge KC, Graybiel AM, Fentress JC. Neurobiology of rodent self-grooming and its value for translational neuroscience. Nat Rev Neurosci. 2016 Jan;17(1):45–59.

15. Peixoto RT, Wang W, Croney DM, Kozorovitskiy Y, Sabatini BL. Early hyperactivity and precocious maturation of corticostriatal circuits in Shank3B â ’/â ’ mice. Nat Neurosci. 2016;

16. Bey AL, Wang X, Yan H, Kim N, Passman RL, Yang Y, et al. Brain region-specific disruption of Shank3 in mice reveals a dissociation for cortical and striatal circuits in autism-related behaviors. Transl Psychiatry. 2018 Dec;8(1):94.

17. Jin C, Lee Y, Kang H, Jeong K, Park J, Zhang Y, et al. Increased ribosomal protein levels and protein synthesis in the striatal synaptosome of Shank3-overexpressing transgenic mice. Mol Brain. 2021 Feb 23;14(1):39.

18. Reim D, Distler U, Halbedl S, Verpelli C, Sala C, Bockmann J, et al. Proteomic Analysis of Post-synaptic Density Fractions from Shank3 Mutant Mice Reveals Brain Region Specific Changes Relevant to Autism Spectrum Disorder. Front Mol Neurosci. 2017 Feb;10:26.

19. Schoen M, Asoglu H, Bauer HF, Müller H-P, Abaei A, Sauer AK, et al. Shank3 Transgenic and Prenatal Zinc-Deficient Autism Mouse Models Show Convergent and Individual Alterations of Brain Structures in MRI. Front Neural Circuits. 2019;13:6.

20. Wang W, Li C, Chen Q, Goes M-SS van der, Hawrot J, Yao AY, et al. Striatopallidal dysfunction underlies repetitive behavior in Shank3-deficient model of autism. J Clin Invest. 2017 May;127(5):1978–90.

21. Schmeisser MJ, Ey E, Wegener S, Bockmann J, Stempel AV, Kuebler A, et al. Autistic-like behaviours and hyperactivity in mice lacking ProSAP1/Shank2. Nature. 2012 Apr;486(7402):256–60.

22. R Core Team (R Foundation for Statistical Computing V. R: A language and environment for statistical computing. 2020; Available from: https://www.r-project.org/

23. Park J, Coddington LT, Dudman JT. Basal Ganglia Circuits for Action Specification. Annu Rev Neurosci. 2020 Jul 8;43:485–507.

24. Gokce O, Stanley GM, Treutlein B, Neff NF, Camp JG, Malenka RC, et al. Cellular Taxonomy of the Mouse Striatum as Revealed by Single-Cell RNA-Seq. Cell Rep. 2016 Jul;16(4):1126–37.

25. Montalban E, Giralt A, Taing L, Nakamura Y, Martin C, Pins B de, et al. Translational profiling of mouse dopaminoceptive neurons reveals a role of PGE2 in dorsal striatum [Internet]. 2020 Sep [cited 2021 Nov 24] p. 2020.09.02.279240. Available from: https://www.biorxiv.org/content/10.1101/2020.09.02.279240v1

26. Davis MI, Crittenden JR, Feng AY, Kupferschmidt DA, Naydenov A, Stella N, et al. The cannabinoid-1 receptor is abundantly expressed in striatal striosomes and striosome-dendron bouquets of the substantia nigra. PloS One. 2018;13(2):e0191436.

27. Lévesque M, Wallman M-J, Parent A. Striosomes are enriched in glutamic acid decarboxylase in primates. Neurosci Res. 2004 Sep;50(1):29–35.

28. Rivera A, Cuéllar B, Girón FJ, Grandy DK, de la Calle A, Moratalla R. Dopamine D4 receptors are heterogeneously distributed in the striosomes/matrix compartments of the striatum. J Neurochem. 2002 Jan;80(2):219–29.

29. Sako W, Morigaki R, Nagahiro S, Kaji R, Goto S. Olfactory type G-protein alpha subunit in striosome-matrix dopamine systems in adult mice. Neuroscience. 2010 Oct 13;170(2):497–502.

30. Miyamoto Y, Katayama S, Shigematsu N, Nishi A, Fukuda T. Striosome-based map of the mouse striatum that is conformable to both cortical afferent topography and uneven distributions of dopamine D1 and D2 receptor-expressing cells. Brain Struct Funct. 2018 Dec;223(9):4275–91.

31. Pagani M, Bertero A, Liska A, Galbusera A, Sabbioni M, Barsotti N, et al. Deletion of Autism Risk Gene Shank3 Disrupts Prefrontal Connectivity. J Neurosci Off J Soc Neurosci. 2019 Jul 3;39(27):5299–310.

32. Wang X, Bey AL, Katz BM, Badea A, Kim N, David LK, et al. Altered mGluR5-Homer scaffolds and corticostriatal connectivity in a Shank3 complete knockout model of autism. Nat Commun. 2016 May;7:11459.

33. Yoo Y-E, Yoo T, Lee S, Lee J, Kim D, Han H-M, et al. Shank3 Mice Carrying the Human Q321R Mutation Display Enhanced Self-Grooming, Abnormal Electroencephalogram Patterns, and Suppressed Neuronal Excitability and Seizure Susceptibility. Front Mol Neurosci. 2019;12:155.

34. de Chaumont F, Lemière N, Coqueran S, Bourgeron T, Ey E. LMT USV Toolbox, a Novel Methodological Approach to Place Mouse Ultrasonic Vocalizations in Their Behavioral Contexts-A Study in Female and Male C57BL/6J Mice and in Shank3 Mutant Females. Front Behav Neurosci. 2021;15:735920.

35. Ey E, Torquet N, Chaumont F de, Lévi-Strauss J, Ferhat A-T, Sourd A-ML, et al. Shank2 Mutant Mice Display Hyperactivity Insensitive to Methylphenidate and Reduced Flexibility in Social Motivation, but Normal Social Recognition. Front Mol Neurosci [Internet]. 2018 Oct;11. Available from: /pmc/articles/PMC6180161/ /pmc/articles/PMC6180161/?report=abstract https://www.ncbi.nlm.nih.gov/pmc/articles/PMC6180161/ https://www.frontiersin.org/article/10.3389/fnmol.2018.00365/full

36. Bariselli S, Tzanoulinou S, Glangetas C, Prévost-Solié C, Pucci L, Viguié J, et al. SHANK3 controls maturation of social reward circuits in the VTA. Nat Neurosci. 2016 Jul;19(7):926–34.

37. Bariselli S, Bellone C. VTA DA neuron excitatory synapses in Shank3 Δex4–9mouse line. Synapse. 2017;71(6):1–5.

38. Orefice LL, Mosko JR, Morency DT, Wells MF, Tasnim A, Mozeika SM, et al. Targeting Peripheral Somatosensory Neurons to Improve Tactile-Related Phenotypes in ASD Models. Cell. 2019 Aug 8;178(4):867-886.e24.

39. Lin R, Learman LN, Bangash MA, Melnikova T, Leyder E, Reddy SC, et al. Homer1a regulates Shank3 expression and underlies behavioral vulnerability to stress in a model of Phelan-McDermid syndrome. Cell Rep. 2021 Nov 16;37(7):110014.

40. Qin L, Ma K, Wang Z-J, Hu Z, Matas E, Wei J, et al. Social deficits in Shank3-deficient mouse models of autism are rescued by histone deacetylase (HDAC) inhibition. Nat Neurosci [Internet]. 2018 Mar; Available from: http://www.ncbi.nlm.nih.gov/pubmed/29531362 http://www.nature.com/articles/s41593-018-0110-8

41. Moutin E, Sakkaki S, Compan V, Bouquier N, Giona F, Areias J, et al. Restoring glutamate receptosome dynamics at synapses rescues autism-like deficits in Shank3-deficient mice. Mol Psychiatry. 2021 Jul 30;1–14.

42. Chen Y-W, Lin H-C, Ng M-C, Hsiao Y-H, Wang C-C, Gean P-W, et al. Activation of mGluR2/3 underlies the effects of N-acetylcystein on amygdala-associated autism-like phenotypes in a valproate-induced rat model of autism. Front Behav Neurosci. 2014 Jun;8:219.

43. Boeckers TM, Inter C, Smalla KH, Kreutz MR, Bockmann J, Seidenbecher C, et al. Proline-rich synapse-associated proteins ProSAP1 and ProSAP2 interact with synaptic proteins of the SAPAP/GKAP family. Biochem Biophys Res Commun. 1999;264(1):247–52.

44. Gogolla N, Takesian AE, Feng G, Fagiolini M, Hensch TK. Sensory integration in mouse insular cortex reflects GABA circuit maturation. Neuron. 2014 Aug 20;83(4):894–905.

45. Litvin Y, Phan A, Hill MN, Pfaff DW, McEwen BS. CB1 receptor signaling regulates social anxiety and memory. Genes Brain Behav. 2013;12(5):479–89.

46. Tallett AJ, Blundell JE, Rodgers RJ. Endogenous opioids and cannabinoids: system interactions in the regulation of appetite, grooming and scratching. Physiol Behav. 2008 Jun 9;94(3):422–31.

47. Terzian AL, Drago F, Wotjak C, Micale V. The Dopamine and Cannabinoid Interaction in the Modulation of Emotions and Cognition: Assessing the Role of Cannabinoid CB1 Receptor in Neurons Expressing Dopamine D1 Receptors. Front Behav Neurosci. 2011;5:49.

48. Folkes OM, Báldi R, Kondev V, Marcus DJ, Hartley ND, Turner BD, et al. An endocannabinoid-regulated basolateral amygdala-nucleus accumbens circuit modulates sociability. J Clin Invest. 2020 Apr 1;130(4):1728–42.

49. Zou M, Liu Y, Xie S, Wang L, Li D, Li L, et al. Alterations of the endocannabinoid system and its therapeutic potential in autism spectrum disorder. Open Biol. 2021 Feb;11(2):200306.

50. Pelosi A, Menardy F, Popa D, Girault J-A, Hervé D. Heterozygous Gnal Mice Are a Novel Animal Model with Which to Study Dystonia Pathophysiology. J Neurosci. 2017 Jun 28;37(26):6253–67.

51. Lee B, Zhang Y, Kim Y, Kim S, Lee Y, Han K. Age-dependent decrease of GAD65/67 mRNAs but normal densities of GABAergic interneurons in the brain regions of Shank3 -overexpressing manic mouse model. Neurosci Lett. 2017 May;649:48–54.

52. Hagimoto K, Takami S, Murakami F, Tanabe Y. Distinct migratory behaviors of striosome and matrix cells underlying the mosaic formation in the developing striatum. J Comp Neurol. 2017 Mar 1;525(4):794–817.

53. Crittenden J, Graybiel A. Basal Ganglia Disorders Associated with Imbalances in the Striatal Striosome and Matrix Compartments. Front Neuroanat. 2011;5:59.

54. Prager EM, Plotkin JL. Compartmental function and modulation of the striatum. J Neurosci Res. 2019 Dec;97(12):1503–14.

55. Prager EM, Dorman DB, Hobel ZB, Malgady JM, Blackwell KT, Plotkin JL. Dopamine Oppositely Modulates State Transitions in Striosome and Matrix Direct Pathway Striatal Spiny Neurons. Neuron. 2020 Dec 23;108(6):1091-1102.e5.

56. Jaquins-Gerstl A, Nesbitt KM, Michael AC. In vivo evidence for the unique kinetics of evoked dopamine release in the patch and matrix compartments of the striatum. Anal Bioanal Chem. 2021 Nov;413(27):6703–13.

57. Friedman A, Homma D, Bloem B, Gibb LG, Amemori K-I, Hu D, et al. Chronic Stress Alters Striosome-Circuit Dynamics, Leading to Aberrant Decision-Making. Cell. 2017 Nov 16;171(5):1191-1205.e28.

58. Canales JJ, Graybiel AM. A measure of striatal function predicts motor stereotypy. Nat Neurosci. 2000 Apr;3(4):377–83.

59. Murray RC, Logan MC, Horner KA. Striatal patch compartment lesions reduce stereotypy following repeated cocaine administration. Brain Res. 2015 Aug 27;1618:286–98.

60. Karunakaran KB, Amemori S, Balakrishnan N, Ganapathiraju MK, Amemori K. Generalized and social anxiety disorder interactomes show distinctive overlaps with striosome and matrix interactomes. Sci Rep. 2021 Sep 15;11(1):18392.

61. Friedman A, Homma D, Gibb LG, Amemori K, Rubin SJ, Hood AS, et al. A Corticostriatal Path Targeting Striosomes Controls Decision-Making under Conflict. Cell. 2015 Jun 4;161(6):1320–33.

62. Friedman A, Hueske E, Drammis SM, Toro Arana SE, Nelson ED, Carter CW, et al. Striosomes Mediate Value-Based Learning Vulnerable in Age and a Huntington's Disease Model. Cell. 2020 Nov 12;183(4):918-934.e49.

63. Nadel JA, Pawelko SS, Scott JR, McLaughlin R, Fox M, Ghanem M, et al. Optogenetic stimulation of striatal patches modifies habit formation and inhibits dopamine release. Sci Rep. 2021 Oct 6;11(1):19847.

64. Kuo H-Y, Liu F-C. Valproic acid induces aberrant development of striatal compartments and corticostriatal pathways in a mouse model of autism spectrum disorder. FASEB J. 2017;31(10):4458–71.

65. Kuo H-Y, Liu F-C. Pathological alterations in striatal compartments in the human brain of autism spectrum disorder. Mol Brain. 2020 Dec;13(1):83.

66. Esclapez M, Tillakaratne NJ, Kaufman DL, Tobin AJ, Houser CR. Comparative localization of two forms of glutamic acid decarboxylase and their mRNAs in rat brain supports the concept of functional differences between the forms. J Neurosci Off J Soc Neurosci. 1994 Mar;14(3 Pt 2):1834–55.

67. Kaufman DL, Houser CR, Tobin AJ. Two forms of the gamma-aminobutyric acid synthetic enzyme glutamate decarboxylase have distinct intraneuronal distributions and cofactor interactions. J Neurochem. 1991 Feb;56(2):720–3.

68. Watabe-Uchida M, Zhu L, Ogawa SK, Vamanrao A, Uchida N. Whole-brain mapping of direct inputs to midbrain dopamine neurons. Neuron. 2012 Jun 7;74(5):858–73.

69. McGregor MM, McKinsey GL, Girasole AE, Bair-Marshall CJ, Rubenstein JLR, Nelson AB. Functionally Distinct Connectivity of Developmentally Targeted Striosome Neurons. Cell Rep. 2019 Nov 5;29(6):1419-1428.e5.

70. Jaramillo TC, Xuan Z, Reimers JM, Escamilla CO, Liu S, Powell CM. Early Restoration of Shank3 Expression in Shank3 Knock-Out Mice Prevents Core ASD-Like Behavioral Phenotypes. eNeuro. 2020 Jun;7(3):ENEURO.0332-19.2020.

71. Huang G, Chen S, Chen X, Zheng J, Xu Z, Doostparast Torshizi A, et al. Uncovering the Functional Link Between SHANK3 Deletions and Deficiency in Neurodevelopment Using iPSC-Derived Human Neurons. Front Neuroanat. 2019 Mar 13;13:23.

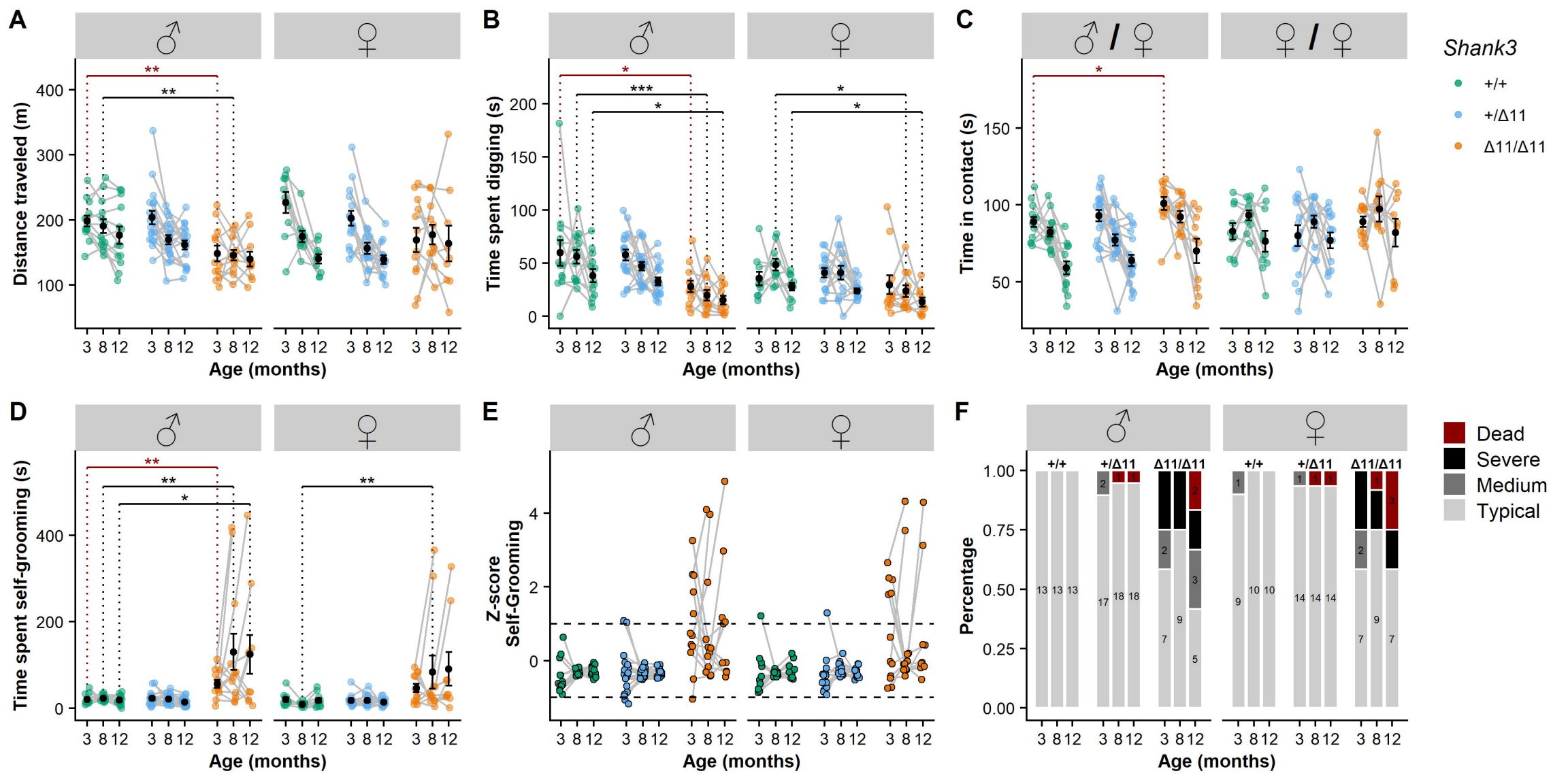
A
B
C
D
E
F
♂
♀
♂ / ♀
♀ / ♀
Distance traveled (m)
Time spent digging (s)
Time in contact (s)
Time spent self-grooming (s)
Z-score Self-Grooming
Percentage
Age (months)
Shank3
+/+
+/Δ11
Δ11/Δ11
Dead
Severe
Medium
Typical

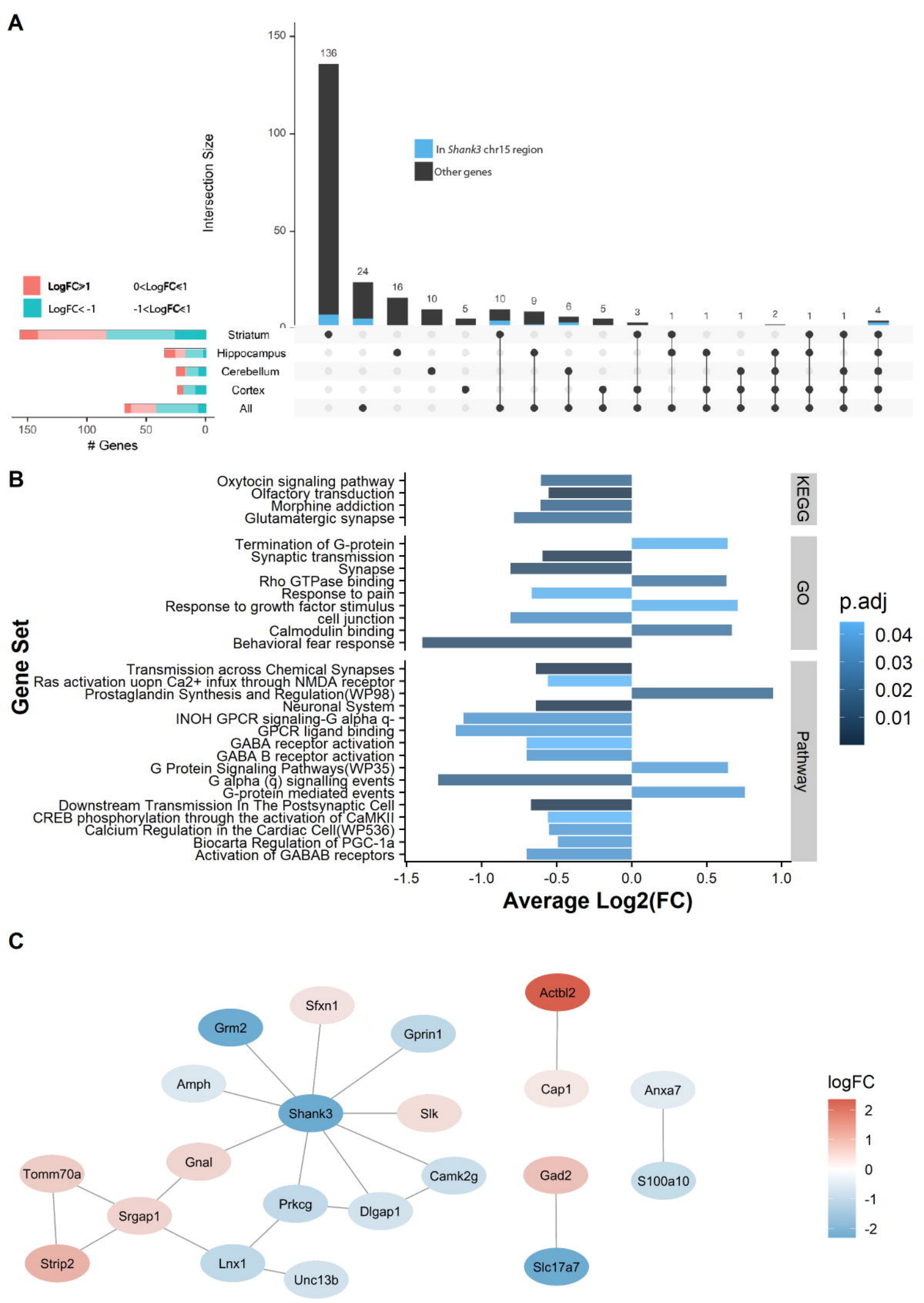
A
Intersection Size
In Shank3 chr15 region
Other genes
LogFC≥1
0<LogFC≤1
LogFC< -1
-1<LogFC≤1
Striatum
Hippocampus
Cerebellum
Cortex
All
Genes
B
Gene Set
KEGG
GO
Pathway
Oxytocin signaling pathway
Olfactory transduction
Morphine addiction
Glutamatergic synapse
Termination of G-protein
Synaptic transmission
Synapse
Rho GTPase binding
Response to pain
Response to growth factor stimulus
cell junction
Calmodulin binding
Behavioral fear response
Transmission across Chemical Synapses
Ras activation uopn Ca2+ infux through NMDA receptor
Prostaglandin Synthesis and Regulation(WP98)
Neuronal System
INOH GPCR signaling-G alpha q-
GPCR ligand binding
GABA receptor activation
GABA B receptor activation
G Protein Signaling Pathways(WP35)
G alpha (q) signalling events
G-protein mediated events
Downstream Transmission In The Postsynaptic Cell
CREB phosphorylation through the activation of CaMKII
Calcium Regulation in the Cardiac Cell(WP536)
Biocarta Regulation of PGC-1a
Activation of GABAB receptors
Average Log2(FC)
p.adj
C
Sfxn1
Grm2
Gprin1
Amph
Shank3
Slk
Gnal
Tomm70a
Camk2g
Srgap1
Prkcg
Dlgap1
Strip2
Lnx1
Unc13b
Actbl2
Cap1
Anxa7
Gad2
S100a10
Slc17a7
logFC

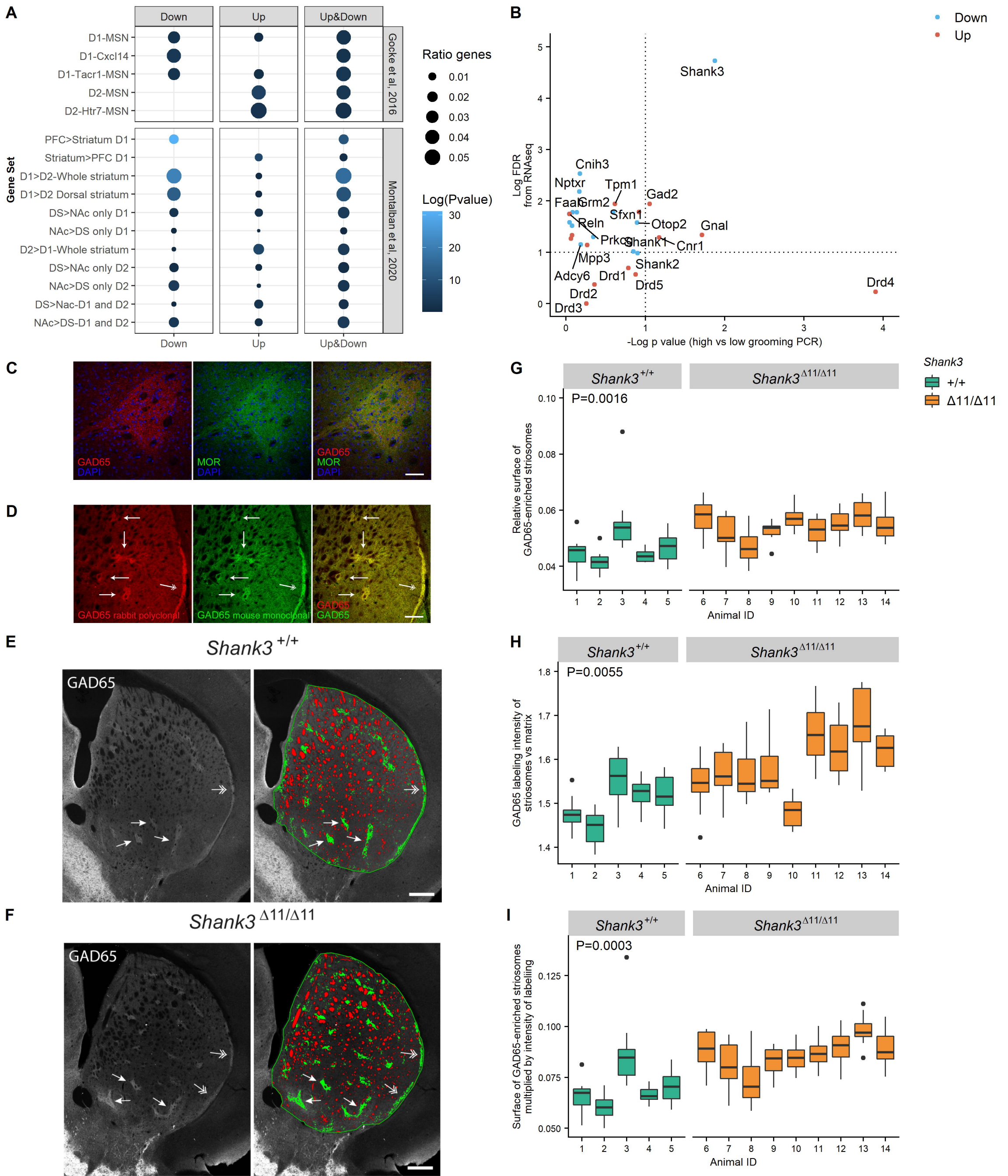
A
Down
Up
Up&Down
D1-MSN
D1-Cxcl14
D1-Tacr1-MSN
D2-MSN
D2-Htr7-MSN
Gocke et al, 2016
PFC>Striatum D1
Striatum>PFC D1
D1>D2-Whole striatum
D1>D2 Dorsal striatum
DS>NAc only D1
NAc>DS only D1
D2>D1-Whole striatum
DS>NAc only D2
NAc>DS only D2
DS>Nac-D1 and D2
NAc>DS-D1 and D2
Montalban et al, 2020
Gene Set
Ratio genes
0.01
0.02
0.03
0.04
0.05
Log(Pvalue)
30
20
10
B
Down
Up
Log FDR from RNAseq
-Log p value (high vs low grooming PCR)
Shank3
Cnih3
Nptxr
Tpm1
Gad2
Grm2
Sfxn1
Reln
Otop2
Gnal
Shank1
Cnr1
Mpp3
Shank2
Adcy6
Drd1
Drd5
Drd4
Drd2
Drd3
C
GAD65
DAPI
MOR
DAPI
GAD65
MOR
DAPI
D
GAD65 rabbit polyclonal
GAD65 mouse monoclonal
GAD65
GAD65
E
Shank3 +/+
GAD65
F
Shank3 Δ11/Δ11
GAD65
G
Shank3+/+
Shank3Δ11/Δ11
P=0.0016
Relative surface of GAD65-enriched striosomes
Animal ID
Shank3
+/+
Δ11/Δ11
H
Shank3+/+
Shank3Δ11/Δ11
P=0.0055
GAD65 labeling intensity of striosomes vs matrix
Animal ID
I
Shank3+/+
Shank3Δ11/Δ11
P=0.0003
Surface of GAD65-enriched striosomes multiplied by intensity of labeling
Animal ID

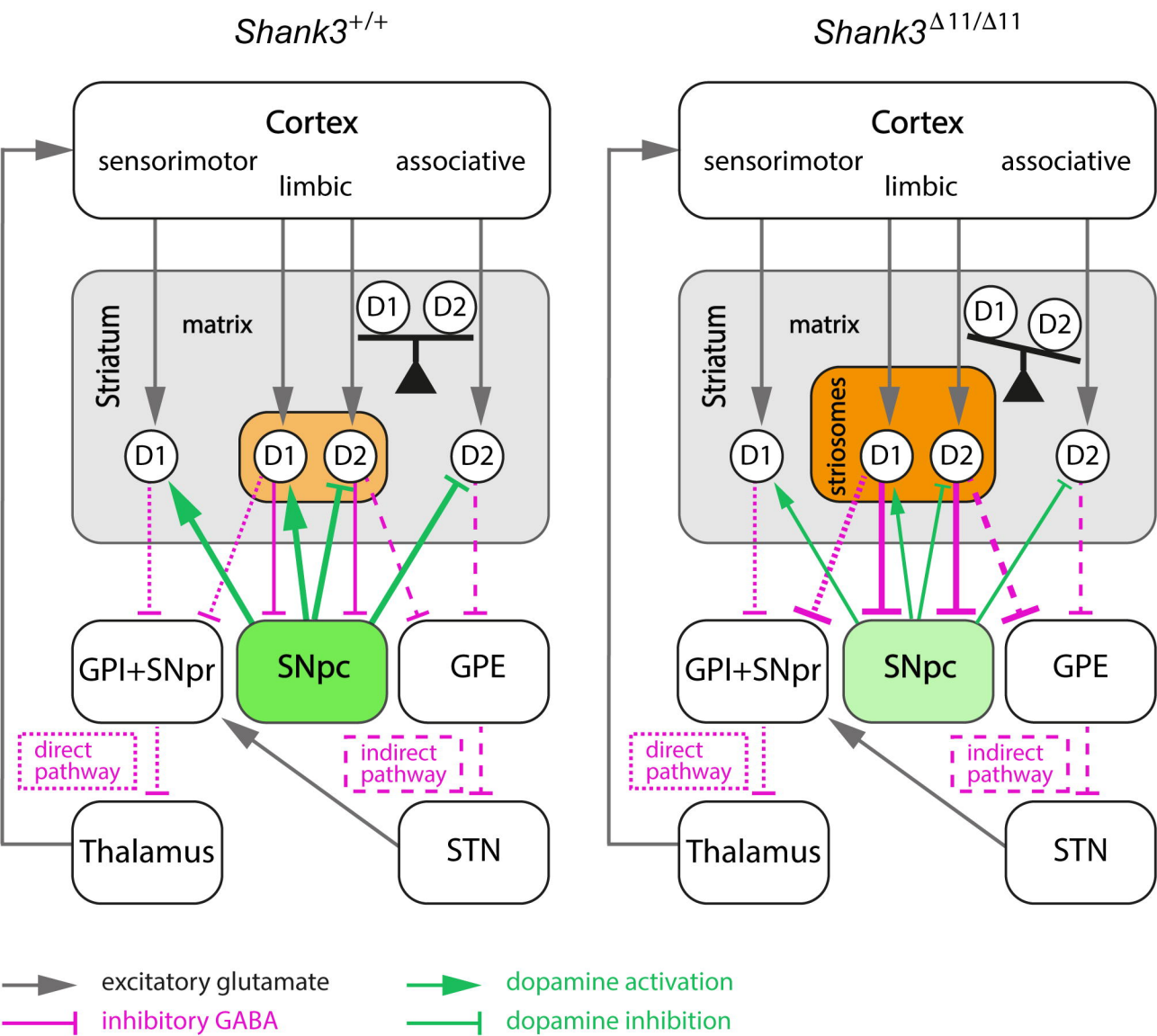
Shank3+/+
Shank3Δ11/Δ11
Cortex
sensorimotor
limbic
associative
Striatum
matrix
striosomes
D1
D2
GPI+SNpr
SNpc
GPE
direct pathway
indirect pathway
Thalamus
STN
excitatory glutamate
inhibitory GABA
dopamine activation
dopamine inhibition